applied sciences

MDPI

Article

The Role of Synergies of MWCNTs and Carbon Black in the Enhancement of the Electrical and Mechanical Response of Modified Epoxy Resins

Georgios Foteinidis, Kyriaki Tsirka, Lazaros Tzounis, Dimitrios Baltzis and Alkiviadis S. Paipetis *

Materials Science & Engineering Department, University of Ioannina, 45110 Ioannina, Greece
* Correspondence: paipetis@uoi.gr; Tel.: +30-26510-08001

Received: 24 July 2019; Accepted: 4 September 2019; Published: 8 September 2019

Featured Application: This work was focused on the modification of the epoxy matrix so as to produce nanocomposites with enhanced electrical and mechanical properties. With respect to the specific application, these nanocomposites may be employed independently or as matrices for multi-functional composite materials employed in various sectors such as the energy, the automotive or the aerospace sector. Apart from enhanced mechanical properties, through nanomodification, a variety of additional functionalities may be imparted to the structure, ranging from antistatic properties and strain sensing to structural health monitoring, electromagnetic shielding, energy harvesting and storage, actuation and morphing.

Abstract: Nano-reinforced composites are widely studied by the scientific community. The main factors affecting the final nanocomposite performance are the filler type and content, as well as the duration of the dispersion. In this work, we report the effects of Multi-Walled Carbon Nano Tubes (MWCNTs) and milled Carbon Black (CB) dispersion in epoxy resin on the electrical and mechanical properties of the resulting composites. Impedance Spectroscopy (IS) was utilized to assess the dielectric properties of the specimens. The mechanical properties were evaluated by fracture toughness tests, while Scanning Electron Microscopy (SEM) was performed to study the influence of the reinforcement on the failure mechanisms acting on the fracture surfaces of the specimens. IS results for epoxy/CNT systems revealed the creation of a 3D conductive network for concentrations above 0.3 wt. %, while CB did not result in the formation of such a network for filler contents up to 2 wt. %. However, the synergistic effect of CNTs/CB was successfully manifested by both the optimal electrical properties and the 81% enhanced fracture toughness in comparison to the neat resin. Fractography confirmed the aforementioned results and revealed the fracture mechanisms of all systems, such as crack pinning and deflection, and particle pull-out phenomena.

Keywords: nanocomposites; hybrid composites; impedance spectroscopy; fracture toughness; fractography

1. Introduction

Since their discovery by Prileschajew in 1909, epoxy resins have found a wide range of applications [1]. Due to their exceptional mechanical properties, which include high adhesive strength, high electrical insulation and good heat resistance, epoxy resins are used as coatings, adhesives and matrices for fiber-reinforced polymer (FRP) composites in demanding engineering fields such as the aerospace, naval, and automotive industries, etc. [2–5]. Despite the exceptional mechanical and physical properties of epoxy resins, their highly dielectric character creates a barrier to the addition

of functionalities such as strain sensing and Structural Health Monitoring (SHM), where electrical conductivity of the material is demanded [6–11].

It is well known that the addition of a nano- or micro-scaled conductive phase inside the insulating epoxy matrix is capable of increasing the electrical and thermal conductivity, as well as improving the mechanical properties [12]. According to various studies, some of the most promising carbonaceous nano-fillers include carbon nanotubes (CNTs), due to their unique 1D character and extremely high aspect ratio (L/d), and graphene; meanwhile, short carbon fibers and Carbon Black (CB) are the most widely used micro-scale fillers [12–14].

Polymer nanocomposites are attractive materials due to their ease of production, relatively low cost, environmentally benign characteristics, flexibility, and high specific properties [15–19]. The introduction of CNTs in engineering thermosetting, thermoplastic and elastomer polymer-based matrices has resulted in electrically conductive nanocomposites [20–23]. Specifically, the CNT networks in a polymer matrix allow electron transport by a tunneling or a hopping mechanism when junctions are separated by an insulating polymeric film [24]. Fundamental to the attainment of these properties is the concentration of the filler exceeding a critical concentration, called the percolation threshold. Above this concentration, the formation of a network of the nano- or the micro-filler occurs, and this network is responsible for the charge carrier transport phenomena, which impart electrical conductivity to the matrix [12,25].

A positive side-effect of the introduction of carbonaceous fillers in epoxies is the improved mechanical properties that can be also achieved [12,13]. Such fillers include CB [26,27], and single-, double- or multi-walled carbon nanotubes (SWCNTs, DWCNTs, MWCNTs respectively) [28], and can impart significantly enhanced mechanical properties like flexural strength, facture toughness, adhesion strength, etc. [14,29,30], to epoxy matrices. The magnitude of improvement in material properties is highly dependent on the dispersion efficiency of the fillers in the epoxy resins and parameters like the employed dispersion method, duration or intensity, the filler type and weight content can greatly affect the resulting composite performance [31].

The most important parameter for the deployment of electrical and mechanical properties of CNTs in a CNT polymer nanocomposite is the dispersion process, to achieve an optimum nano-scale CNT disentangled network with extended CNT junctions. As such, the high quality of CNT dispersion can facilitate the full exploitation of the electrical, mechanical, thermal, etc., properties of the CNT nanoparticulate additives, while at the same time preserving an ultra-low percolation threshold. Namely, for epoxy/CNT nanocomposites it is crucial to optimize the time and shear conditions for the shear assisted dispersion of CNTs, while for thermoplastic/CNT nanocomposites, the appropriate melt-mixing conditions and temperature to facilitate polymer infiltration through the CNT macro- and micro- aggregates without degrading the polymer matrix are of utmost importance [12]. It could thus be realized that techniques for the real-time characterization and study of the dispersion state and the quality of the CNT network during processing are essential for optimizing the dispersion process, as well as for the process of quality monitoring control.

Since the nano- and micro-particle dispersion strongly affect the electrical properties of the composite, the results of electrical measurements can be directly connected with dispersion quality. Among numerous DC and AC electrical techniques, Impedance Spectroscopy (IS) utilizes an alternate excitation voltage over a wide range of frequencies, either by frequency sweep or Fast Fourier Transform (FFT). As a response of the material under test to the external field, a current is received to the IS analyzer. The resulting current is compared to the excitation voltage in terms of amplitude and phase delay, offering a complete view of the electrical properties as a function of the frequency of the medium. IS is characterized as a non-destructive technique, and is widely used for curing monitoring of thermosetting epoxy resins, damage analysis and Structural Health Monitoring (SHM) in composite materials [8,32–34].

Another significant application of IS is the conductive nanoparticle dispersion monitoring in the polymeric resin matrix [14,35]. Baltzis et al. studied the effects of dispersion duration and filler type on

the final electrical and mechanical properties of epoxy-based composites. The authors in this study used a two-part epoxy resin system, namely the LY5052 resin and the Aradur 5052 hardener, with Multi Walled Carbon Nano Tubes (MWCNTs) and milled CB. This composite system exhibited improved electrical and mechanical properties due to the exploitation of the synergistic effects of the different scale fillers in comparison to the composites reinforced by a single filler [14]. Furthermore, according to some studies, the enhanced properties of the nanocomposites with the same loading of nano- and micro-materials differs if the host type of the matrix is dissimilar [36,37]. Considering these studies, an alteration of the matrix type may affect the properties of the final composites.

This manuscript is focused on the development of a parametric study of polymeric nanocomposites and hybrid nanocomposites, containing MWCNTs and CB in Diglycidyl Ether of bisphenol-A (DGEBA) epoxy resin, to investigate the effects of the carbon particle dispersion in epoxy resin on the electrical and the mechanical properties. Dispersions were performed using a high-speed shear mixer. IS was utilized to monitor the final dielectric properties of composites produced under various dispersion protocols. These protocols were selected for a comprehensive study of the effects of the filler content and type, including the emergence of possible synergistic effects due to the combination of MWCNTs and CB, as well as the duration of the dispersion process to the final electrical and mechanical properties of the composites. Hence, fracture toughness of the composites was assessed through three-point bending on single edge notched beam specimens (SENB). Finally, Scanning Electron Microscopy (SEM) was utilized to study the failure mechanisms on the fracture surfaces of the SENB specimens regarding the influence of the reinforcement.

2. Materials and Methods

2.1. Materials

Graphistrength C100 Multi Wall CNTs (MWCNTs) supplied by ARKEMA were used as the primary filler in this study. The diameter of the MWCNTs varies between 10 and 15 nm, and the length ranges from 1 μm to 10 μm. The nanotubes were provided in the form of agglomerated bundles with an average diameter of 400 μm with a range of 50 μm to 900 μm. As secondary reinforcement, milled Carbon Black (CB) was provided by R&G composites GmbH with an average agglomerate size ranging from 5 to 50 μm in diameter.

Two parts Diglycidyl Ether of bisphenol-A epoxy resin (DGEBA, Epikote 828 epoxy resin and Epicure 541 hardener) was selected as a matrix, kindly provided by Dichem Polymers, Greece. Weight concentrations of fillers were calculated based on resin-hardener system weight.

2.2. Dispersion Method

All dispersion protocols were performed using a laboratory dissolver device (Dispermat AE by Gentzman) with a double wall vacuum container in combination with a refrigerated thermostatic bath and circulator, provided by GRANT, capable for temperature control within ±1 °C accuracy and dispersion under vacuum conditions. Shear mixing was selected among other dispersion techniques to avoid potential CNT length shortening and degradation of the epoxy polymer matrix. A 45-mm-diameter toothed impeller disk was selected, offering medium shear forces to dispersion, to reduce the agglomerates' size. The conditions of all dispersion protocols were rotary speed at 3000 rounds per minute (rpm) and temperature at 25 °C.

2.3. Dispersion Protocols

The composites employed in this study were manufactured under numerous dispersion protocols with different filler weight content/type and dispersion duration. Two types of systems were manufactured: (i) binary systems, that is, two-part systems, consisting of resin and CNTs or CB; and (ii) ternary systems, that is, three-part systems, where the synergy effects of CNTs and CB in the resin were evaluated. Two binary systems and one ternary system were studied in this work. The first binary

system consisted of CNTs in epoxy resin with concentrations of 0.1 wt. %, 0.3 wt. % and 0.5 wt. %. The second binary system was produced by dispersing three different concentrations of CB, 0.5 wt. %, 1% wt. % and 2 wt. %, in resin. Finally, the ternary system, which consisted of CNT, CB and epoxy resin, was studied in terms of two different concentrations of the fillers, 0.5 wt. % CNTs with 1 wt. % CB and 0.5 wt. % CNTs with 2 wt. % CB. It should be noted that the concentration of the CNTs ranges from 0.1 wt. % to 0.5 wt. %. Preliminary studies with the specific epoxy system showed that the concentration of 0.5 wt. % CNTs is an upper limit as, beyond this concentration the increased viscosity makes the system almost unusable. At the same time, CB concentration above 2 wt. % did not alter the electrical behavior of the system. Additionally, as previous studies have indicated [14,30], electrical percolation is reached at ca. 0.5 wt. % CNTs [14]. To this end, a maximum concentration of 0.5 wt. % was chosen for CNTs and 2 wt. % was chosen for CB.

The aforementioned concentrations were also studied regarding the dispersion duration. This is a critical parameter for defining the optimal mixing duration as two mechanisms take place during the dispersion process. Initially, the de-agglomeration of the agglomerates, which is the desired result of the process, occurs. On the other hand, the structural degradation of the fillers could lead to a decrease of the mechanical and the electrical properties of the composite. The dispersion duration studied for each system ranged from 1 to 4 h, with a step of 1 h. A more analytical review of the filler content and dispersion duration is presented in Table 1.

Table 1. Analytical presentation of dispersion protocols.

Group	Sample Name	Dispersion Duration (h)	CNTs (wt. %)	CB (wt. %)
Binary 1	CNTs0.1-I	1	0.1	
	CNTs0.1-II	2	0.1	
	CNTs0.1-III	3	0.1	
	CNTs0.1-IV	4	0.1	
	CNTs0.3-I	1	0.3	
	CNTs0.3-II	2	0.3	
	CNTs0.3-III	3	0.3	
	CNTs0.3-IV	4	0.3	
	CNTs0.5-I	1	0.5	
	CNTs0.5-II	2	0.5	
	CNTs0.5-III	3	0.5	
	CNTs0.5-IV	4	0.5	
Binary 2	CB0.5-I	1		0.5
	CB0.5-II	2		0.5
	CB0.5-III	3		0.5
	CB0.5-IV	4		0.5
	CB1-I	1		1
	CB1-II	2		1
	CB1-III	3		1
	CB1-IV	4		1
	CB2-I	1		2
	CB2-II	2		2
	CB2-III	3		2
	CB2-IV	4		2
Ternary	CNTs0.5_CB1-I	1	0.5	1
	CNTs0.5_CB1-II	2	0.5	1
	CNTs0.5_CB1-III	3	0.5	1
	CNTs0.5_CB1-IV	4	0.5	1
	CNTs0.5_CB2-I	1	0.5	2
	CNTs0.5_CB2-II	2	0.5	2
	CNTs0.5_CB2-III	3	0.5	2
	CNTs0.5_CB2-IV	4	0.5	2

2.4. Manufacturing of Test Specimens

After filler dispersion in epoxy resin, single-edge notched beam specimens (SENB), with dimensions 52 mm × 12 mm × 4 mm, were manufactured and investigated in terms of fracture toughness. For all systems, the modified epoxy resin Epikote 828 was mixed with Epikure 541 hardener at a 100:50 ratio by hand. The mixture was degassed three times for 1 min. at a laboratory vacuum oven and casted into silicon rubber molds. Curing took place for 24 h at 25 °C. A laboratory grinding apparatus was used to ensure that specimens have the desired dimensions and minimize any surface defects. Specimens were left to dry for 24 h at 25 °C to avoid any deterioration at IS measurements. For each dispersion protocol, 6 SENB specimens were manufactured while 3 of them were tested with IS before mechanical testing.

2.5. Characterization Techniques

2.5.1. Impedance Spectroscopy

In Impedance Spectroscopy technique, a sinusoidal voltage is applied to the material under test. The excitation signal has the form of Equation (1).

$$E_t = E_0 \sin(\omega t) \quad (1)$$

where E_t(V) is the voltage at a specific time, E_0(V) is the voltage amplitude and ω(rad/s) is the angular velocity. The relation between angular velocity and frequency (f) is described by the equation $\omega = 2\pi f$.

The applied excitation forces the conductivity mechanisms to adapt to the external field. These mechanisms are divided into three categories, (i) dipole relaxation which occurs from the orientational movement of the dipolar respecting to the excitation field, (ii) electrical conduction due to free electron or ion migration, and (iii) interfacial polarization. Interfacial polarization arises from trapped free charges in the interfacial areas between two phases (e.g., polymeric matrix and reinforcement at composite materials).

Therefore, forcing the excitation field through a dielectric material results in an output current of the same frequency with a phase delay φ which is described by Equation (2).

$$I_t = I_0 \sin(\omega t + \varphi) \quad (2)$$

Finally, the impedance can be estimated by applying an expression analogue to Ohm's general law for direct current R = E/I; Equation (3).

$$Z = \frac{E_t}{I_t} = \frac{E_0 \sin(\omega t)}{I_0 \sin(\omega t + \varphi)} = |Z| \frac{\sin(\omega t)}{\sin(\omega t + \varphi)} \quad (3)$$

Impedance measurements were performed using the Advanced Dielectric Thermal Analysis System (DETA-SCOPE) supplied by ADVISE, Greece. The specimens were placed between two parallel copper plates with dimensions of 52 mm × 12 mm. A sinusoidal voltage of 10 V was applied to the capacitor. Scans were performed between two frequency values (0.01 Hz to 100 kHz) at 14 different frequencies with the duration of each scan to be approximately 275 s. All measurements were performed under stable temperature of 21 ± 0.1 °C controlled by an EXTECH VIR50 IR thermometer. The experimental setup for the impedance spectroscopy measurements is schematically illustrated in Figure 1.

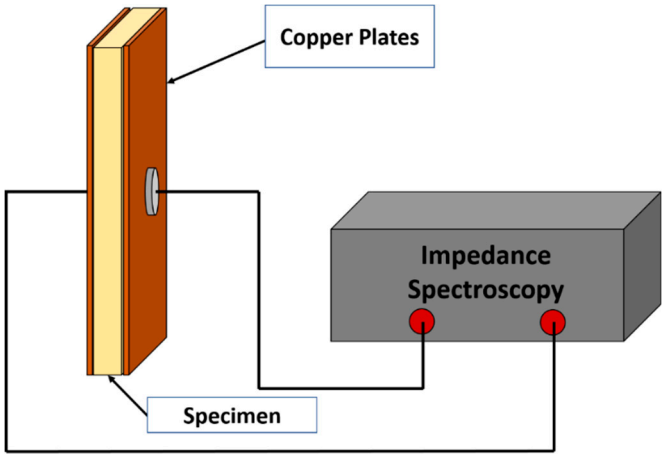

Figure 1. Experimental setup for the impedance spectroscopy measurements.

2.5.2. Fracture Toughness Test

SENB 3-point bending fracture toughness tests were performed according to ASTM D 5045 [38]. Prior to the mechanical testing, a starter crack was created using a metal saw and a fresh razor blade. Specimens were tested using an in-house custom-made horizontal bending stage, while the displacement rate was selected at 1 mm/min. The critical stress intensity factor, K_{ic}, and the energy per unit area of the crack surface or critical strain energy release rate, G_{ic}, were evaluated according to Equations (4) and (5).

$$K_{ic} = \frac{P_{max}}{B \times W^{\frac{1}{2}}} f(x) \quad (4)$$

$$G_{ic} = \frac{U}{B \times W_{\varphi}} \quad (5)$$

where P_{max} is the maximum load, B is the specimen thickness, W is the specimen width, U is the corrected energy under the load vs. deflection curve, and f(x) and φ are calibration factors dependent on the a/W ratio, where a is the crack length.

2.5.3. Fractography via Scanning Electron Microscopy (SEM)

Fractography was performed utilizing SEM and subsequent image analysis using a JEOL JSM 6510LV, Oxford Instruments scanning electron microscope. The selected voltage was 5 kV while the specimens were stabilized on SEM holder with a carbon adhesive tape. Also, specimens were sputter-coated with an Au thin layer to avoid charging effects.

3. Results and Discussion

3.1. Impedance Spectroscopy Results

The addition of conductive fillers in a highly dielectric epoxy matrix can contribute to electrical impedance decrease of the system via a conductive network formation. A fundamental condition to the creation of the conductive network is the concentration of the filler to exceed a critical value, the percolation threshold. IS is a technique capable of monitoring the electric profile of the material under investigation with high sensitivity. The formation of the conductive network is indicated by a steep drop of the magnitude of the impedance by several orders of magnitude. Furthermore, the transition from the Ohmic (linear) to the non-Ohmic (non-linear) behavior of the material, inside the alternative electric field, shifts to higher frequencies.

Figure 2a depicts the dielectric measurements of the whole range of binary and ternary systems after 1 h of the dispersion process. Within the first binary group, the CNTs0.1-I exhibited a frequency-dependent magnitude of impedance, which is a typical dielectric behavior, within the

experimental spectral range. As should be noted, |Z| values above 10^{10} Ohm, at low frequencies, were at the detection limits of the employed setup, hence they presented noise fluctuations.

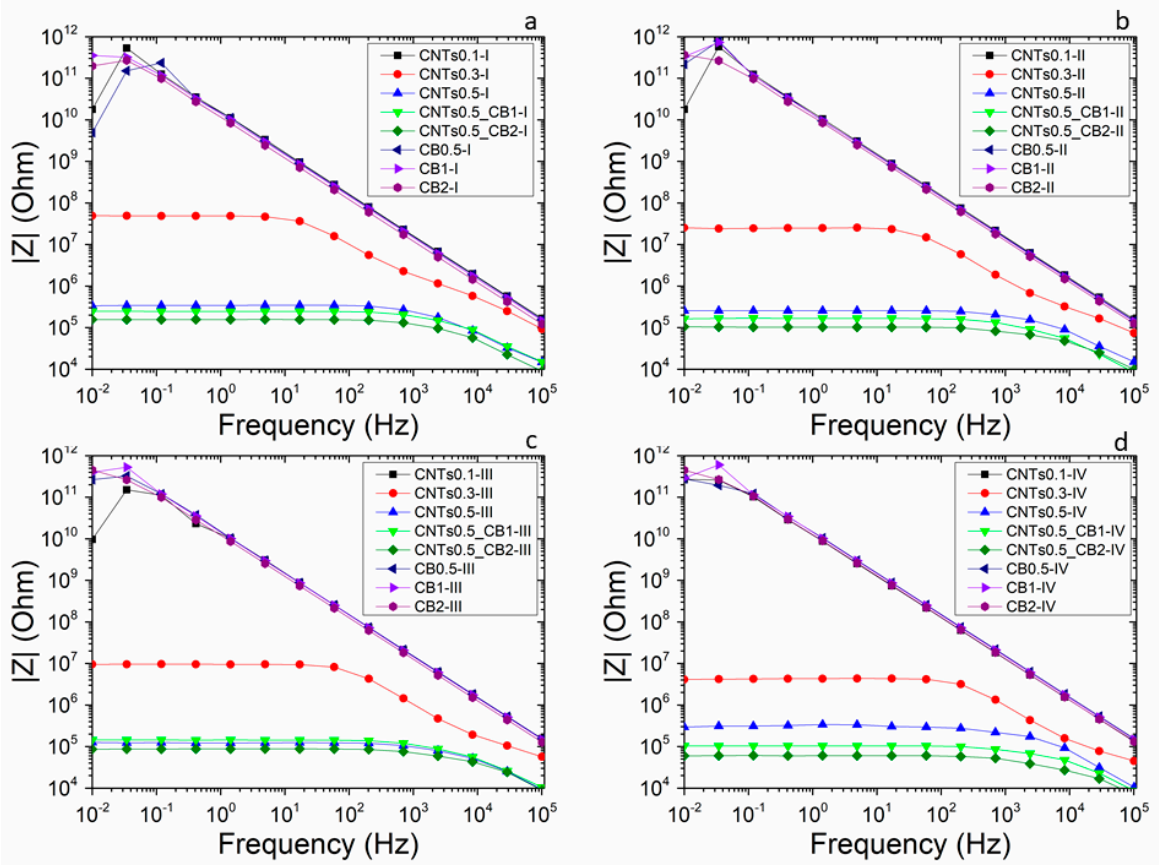

Figure 2. Bode plots of binary and ternary systems for (**a**) 1, (**b**) 2, (**c**) 3 and (**d**) 4 h of dispersion process.

The CNTs0.3-I and the CNTs0.5-I presented a major drop of |Z| after the first hour of the dispersion process (Figure 2a). More specifically, the CNTs0.3-I exhibited a drop by almost 4 orders of magnitude compared to CNTs0.1-I, while the CNTs0.5-I exhibited an even more notable decrease in |Z| by 6 orders of magnitude compared to CNTs0.1-I. This was a clear indicator of the formation of a 3D conductive network. The CNTs0.3-I protocol was sufficient to create a partial network which was fully accomplished at dispersion CNTs0.5-I, defining concentrations between 0.3 wt. % and 0.5 wt. % CNTs as the percolation threshold. Additionally, the transition from the Ohmic (linear) to non-Ohmic (non-linear) behavior shifted from below 10^{-2} Hz for CNTs0.1-I to 10^{1} Hz for CNTs0.3-I, and finally to 10^{3} Hz for the CNTs0.5-I, verifying the conversion of the dielectric character of the nanocomposite to a more conductive one, due to the formation of the conductive network.

The second binary group, consisted of the systems CB0.5-I, CB1-I and CB2-I, which after 1 h of dispersion process, did not present any changes due to the increase of the CB concentration, as the filler content did not exceed the percolation threshold (Figure 2a). The transition from the Ohmic to the non-Ohmic behavior occurred outside the experimental frequency range, below 10^{-2} Hz. These results are in agreement with the literature, which suggests a much higher volume fraction for the formation of a conductive network in CB/resin systems [39]. It should be noted that additional experiments up to 9 wt. % CB did not alter the electrical behavior of the system.

Finally, the ternary group exhibited the optimal electrical properties compared to aforementioned binary systems (Figure 2a). The CNTs0.5_CB2-I protocol presented a slightly more conductive profile from the CNTs0.5_CB1-I, due to the increase of the concentration of CB from 1 wt. % to 2 wt. % and

the synergy with the 0.5 wt. % CNTs. Moreover, the ternary group showed the highest Ohmic to non-Ohmic transition frequency, indicating the worse dielectric profile among all specimens.

Concerning the duration of the dispersion process, among the binary groups, the CNTs0.1-I, the CB0.5-I, the CB1-I and the CB2-I exhibited a stable highly dielectric behavior regarding dispersion time (Figure 2). CNTs0.3-I presented a slight decrease of the impedance indicating the continuous de-agglomeration of the CNTs aggregates during the dispersion process. However, after 4 h of dispersion, the impedance of CNTs0.3-IV (Figure 2d) did not reach the impedance of the specimens with filler content above the percolation threshold. CNTs0.5-I also showed a minor drop of the impedance until the third hour of mixing, followed by an increase after the fourth hour of dispersion by almost half an order of magnitude (Figure 2d). This denoted the structural degradation of the MWCNTs due to extensive dispersion process.

Both ternary systems revealed an almost linear amelioration of their electrical properties in the course of dispersion time, with CNTs0.5_CB2-I being slightly more conductive than CNTs0.5_CB1-I during the progress of dispersion (Figure 2). CNTs0.5_CB2-IV exhibited optimum electrical properties with a magnitude of impedance of about 5×10^4 Ohms, and the transition from Ohmic to non-Ohmic behavior was identified at almost 10^4 Hz (Figure 2d). In conclusion, synergy effects of MWCNTs and CB offered improved electrical properties compared to the binary systems.

3.2. Fracture Toughness

Figures 3–5 illustrate the average values of K_{ic} and G_{ic} for specimens with CNTs and Carbon Black, as well as the Ternary systems for all of the studied dispersion conditions. As can be observed, a general increase in the fracture toughness (K_{ic}) took place for all the systems (binary and ternary). Specifically, G_{ic} increased for the binary systems with CNTs and the ternary systems. However, it remained unaffected within experimental error for the binary systems modified with CB.

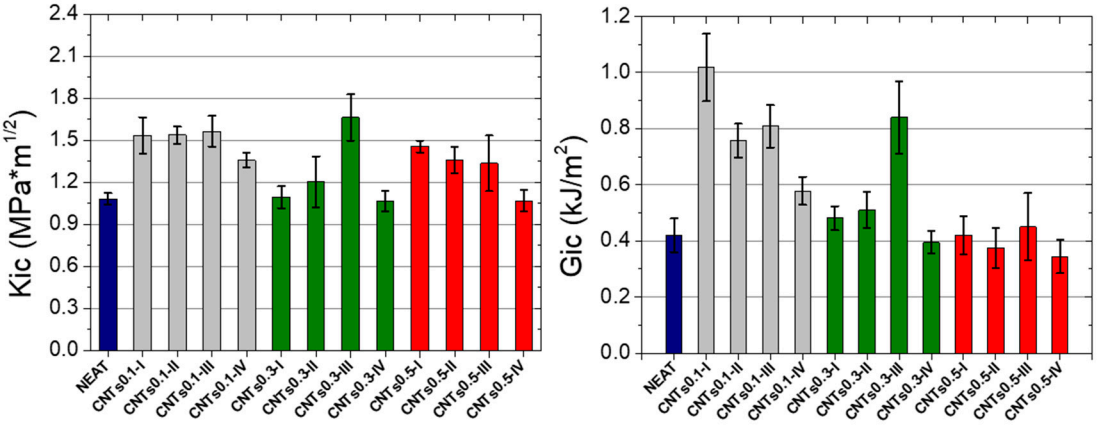

Figure 3. K_{ic} and G_{ic} mean values for specimens with CNTs.

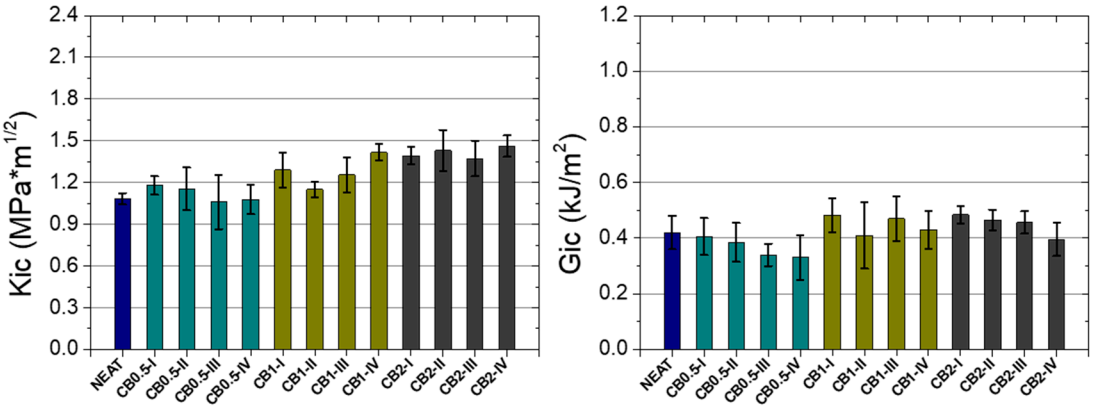

Figure 4. K_{ic} and G_{ic} mean values for specimens with CB.

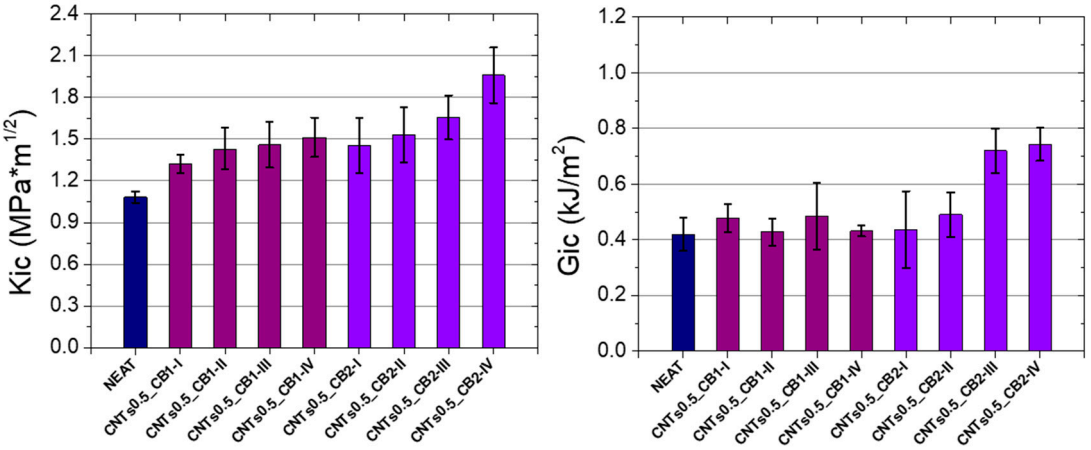

Figure 5. K_{ic} and G_{ic} mean values for ternary specimens.

In more detail, the K_{ic} for the systems with 0.1 wt. % CNTs increased by almost 40% after three hours of dispersion when compared with the neat system, while further dispersion for one more hour led to a deterioration of the average K_{ic} values by ca. 15% for the CNTs0.1-III specimens. This phenomenon can be attributed to the achievement of a threshold at the dispersion duration after which no further improvement can be observed. After the third hour, the agglomerates were eliminated at such an extent that their size could not prevent crack propagation. Similar behavior was exhibited by the specimens with 0.3 wt. % CNTs, which led to a more pronounced increase by 53% after the third hour of dispersion when compared to the neat systems. Conversely, for the specimens with 0.5 wt. % CNTs, only one hour of dispersion was sufficient to cause an almost 34% improvement in K_{ic} while further dispersion led to even lower K_{ic} values.

In terms of G_{ic} values, all systems with CNTs had the same behavior with the K_{ic} values except for CNTs0.1-I, which presented an increase of 142% from the first hour of dispersion. This notable improvement can be attributed to the large scale of agglomerates, which can increase the energy required until the fracture of the specimens. However, for all the CNT modified specimens, the fourth hour of dispersion resulted in a degradation of the G_{ic} values compared to the neat specimens.

In the case of the binary systems with CB, a total increase of the K_{ic} values was observed as the percentage of the filler and the dispersion duration increased (Figure 4). However, when each CB content was examined separately, only small differences in the average K_{ic} values were observed with increasing duration of dispersion, possibly due to the characteristics of the CB. Therefore, no correlation with the dispersion duration was observed for the CB specimens inversely to the case of the CNT modified systems. Furthermore, an amount of 0.5 wt. % CB was found to cause a small

decrease in the average G_{ic} values, while higher CB percentages (1 or 2 wt. %) led to only insignificant increments in the mean G_{ic} values in comparison to the neat system.

Figure 5 presents the mean values of K_{ic} and G_{ic} for the ternary systems. As can be observed, all the ternary systems exhibited a total increase of K_{ic} when compared with the neat systems. The average K_{ic} values increased by 40% after four hours of dispersion for the CNTs0.5_CB1 specimens, while a more pronounced enhancement of about 81% was exhibited by the CNTs0.5_CB2 specimens in comparison to the neat specimens. The combination of the two fillers, which possess nano and micro dimensions, respectively, created a synergetic effect which is capable of hindering crack propagation and producing crack bifurcation phenomena. Moreover, the average G_{ic} values of the CNTs0.5_CB1 were not affected in comparison to the neat specimens. However, a significant improvement by about 65% was observed for the CNTs0.5_CB2-III and the CNTs0.5_CB2-IV systems when compared to the neat specimens.

3.3. Fractographic Study

A fractographic study was also performed on the fracture surfaces of selected SENB specimens to give valuable insights into the failure mechanisms acting on the different systems. Specifically, the binary CNTs0.5-III and CB2-II and the ternary CNTs0.5_CB2-IV specimens with the maximum observed K_{ic} and G_{ic} values were selected for observation and the SEM micrographs are presented in Figures 6–8. A good distribution of the filler particles was observed all over the surfaces of the different systems. However, the morphology of the fractured surfaces differed greatly for each of the binary and the ternary systems.

In more detail, the binary CNTs0.5-III specimen exhibited a rather smooth fracture surface, where only some micro-cracks were evident, indicated by the green circle in Figure 6a. A closer examination revealed the homogenous distribution of the MWCNTs into the resin matrix, as well as the presence of some agglomerated particles (indicated by red circles in Figure 6b). By examining even further the area indicated by the yellow rectangle in Figure 6b, the agglomerates were found to cause crack pinning phenomena (indicated by yellow arrows in Figure 6c) to the secondary generated nano cracks, which are known as tail cracks [40]. Moreover, specific spots were also observed on the fracture surface of the CNTs0.5-III specimen where the network of disentangled CNTs was visible and was accompanied by the presence of agglomerated particles (indicated by the red ellipses in Figure 6d). A closer examination of the CNT network (Figure 6e,f) revealed interconnected long CNT bundles with dimensions with a rough approximation in the range of 50–150 nm. As reported by the manufacturer, the MWCNTs diameter is 10 to 15 nm, and their length is 1 μm to 10 μm and their initial form is that of agglomerated bundles with an average diameter of 400 μm (50 μm to 900 μm). Therefore, the dimensions observed in Figure 6f indicated that these CNT networks were most probably comprised of disentangled bundles of a few CNTs with mostly unaltered length in comparison to their initial state prior to the dispersion process.

A different morphology was observed at the fracture surface of the binary CB2-II specimen, where more and bigger matrix cracks were observed in comparison to the CNTs0.5-III binary specimen. In this case, the crack pinning was the dominant failure mechanism (as indicated by the green circles in Figure 6a,b). Furthermore, particle pull-out and breakage along with void creation, were observed for the CNTs0.5-III binary specimen (as indicated by the blue circles in Figure 6a,b).

Finally, a combination of all the fracture mechanisms which were observed for the binary CNTs0.5-III and the CB2-II specimens were exhibited by the ternary CNTs0.5_CB2-IV specimen. In this case, the simultaneous use of the different scale fillers resulted in the presence of micro-scaled CB particles, micro- and nano-scaled MWCNTs agglomerates, as well as fully disentangled MWCNTs, which were interconnected in a 3D hybrid micro/nano network. This 3D network was capable of impeding crack initiation and propagation more effectively in comparison to the binary systems as indicated by the fracture toughness results, presented above, as well as to cause a more pronounced decrease of the electrical resistivity of the hybrid composite.

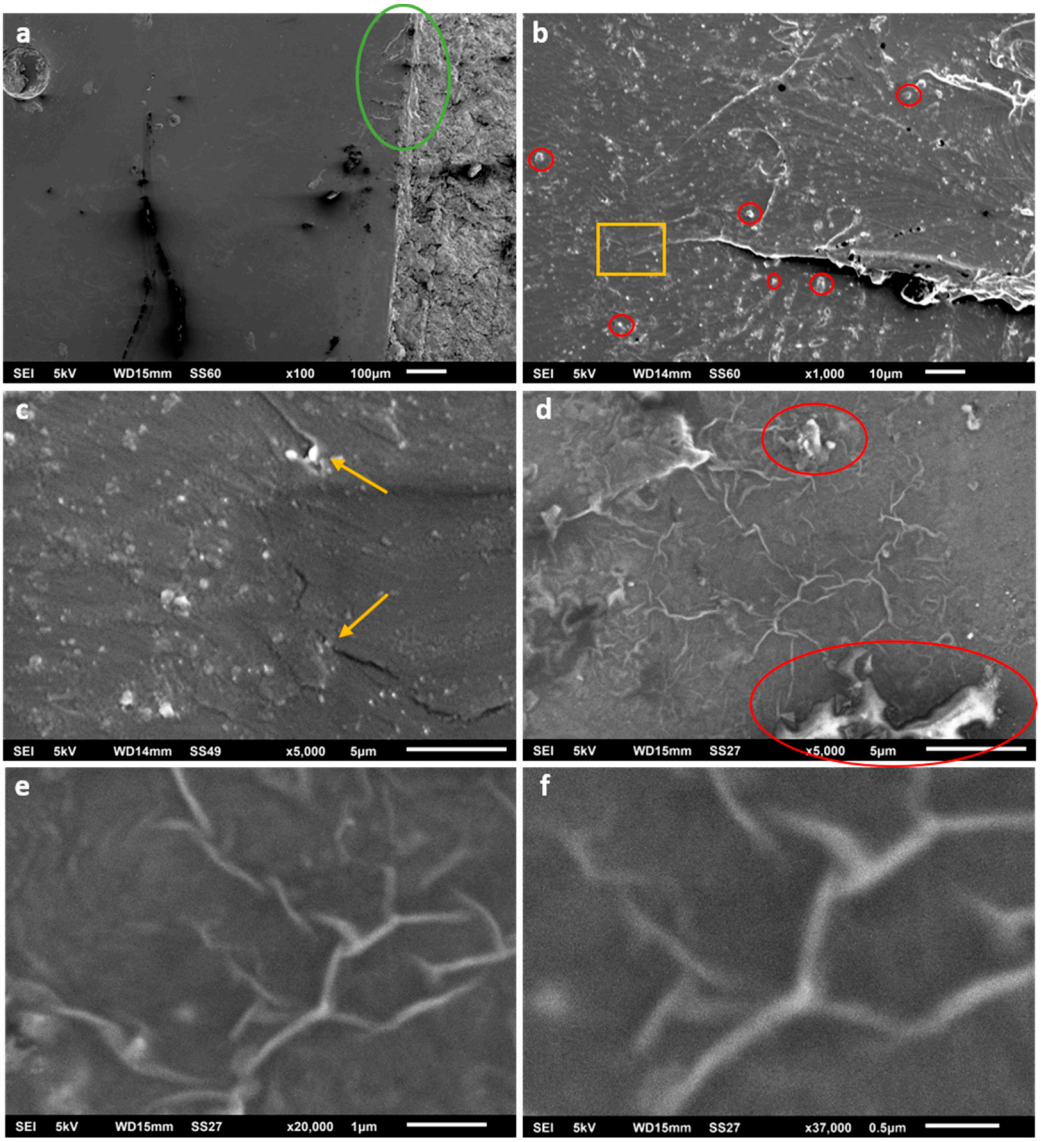

Figure 6. Scanning electron micrographs recorded from the fracture surface of a CNTs0.5-III SENB specimen at (**a**) ×100, (**b**) ×1000, (**c**) and (**d**) ×5000, (**e**) ×20,000, and (**f**) ×37,000 magnification.

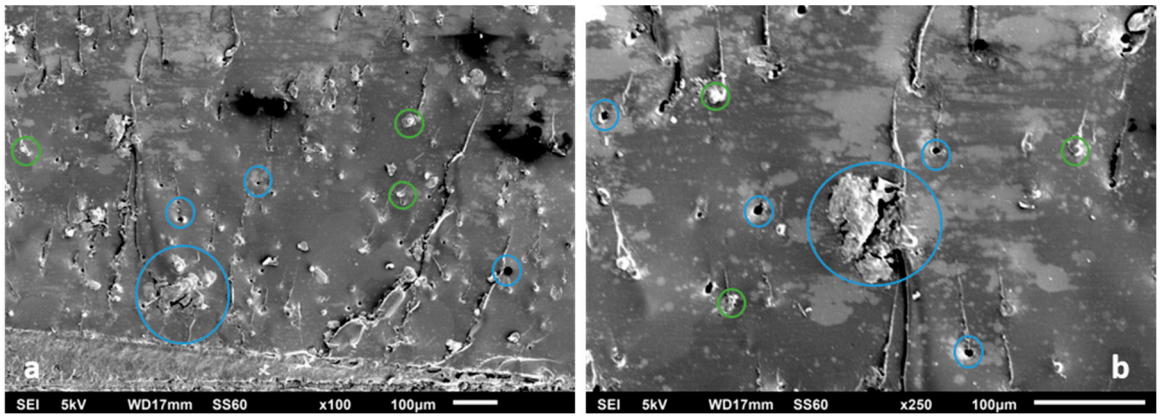

Figure 7. Scanning electron micrographs recorded from the fracture surface of a CB2-IV SENB specimen at (**a**) ×100 and (**b**) ×250 magnifications.

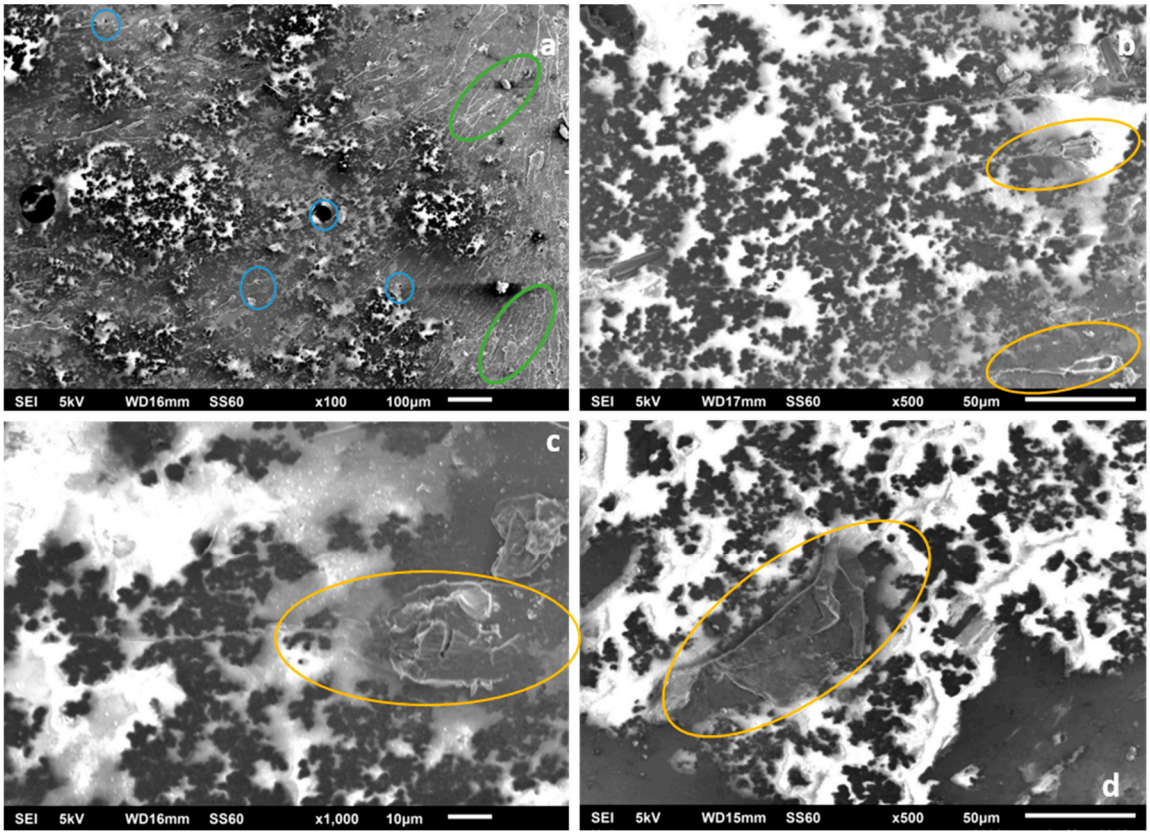

Figure 8. Scanning electron micrographs recorded from the fracture surface of a CNTs0.5_CB2-IV SENB specimen at (**a**) ×100, (**b**) and (**d**) ×500 magnifications, and (**c**) ×1000.

In more detail, both disentangled MWCNTs and CB particles were present in combination with chopped Carbon Fibers (CF) and agglomerated MWCNTs and CB particulates on the fracture surface of the CNTs0.5_CB2-IV specimen. In this case, extended striations, indicative of matrix cracking, were observed (indicated by the green ellipses in Figure 8a), along with the creation of several voids (indicated by the blue circles in Figure 8a) as has also been observed on the fracture surface of the CB2-II specimen. Moreover, crack deflection and crack pinning mechanisms were also in action during the fracture process of the ternary composites (indicated by the yellow ellipsis in Figure 8b–d). Overall, the combination of all these fracture mechanisms led to the pronounced increase in fracture toughness as well as to the notable decrease of the electrical resistivity of the ternary composites in comparison to the binary systems.

4. Conclusions

Within the scope of this work was a study of the effect of CNT and CB dispersions in Diglycidyl Ether of bisphenol-A (DGEBA) epoxy resin on the electrical and mechanical properties. A parametric study was performed to investigate the effects of filler content/type, and dispersion duration by applying IS and mechanical measurements.

IS results for CNT binary protocols indicated the formation of the conductive network for concentrations over 0.3 wt. % MWCNTs, designated by a step drop of impedance magnitude. CNTs0.5_III exhibited optimal electrical properties between CNT binary protocols, while the CNTs0.5_IV showed an increase of the impedance after the fourth hour of dispersion by almost half an order of magnitude, probably caused by CNTs structural degradation. The second binary group consisted of CB dispersion did not present any changes due to the increase of the CB concentration and the dispersion duration. Ternary systems revealed ameliorated electrical properties in comparison to binary systems, manifested by a decrease of the magnitude of the impedance. This behavior was caused

by the synergistic effects of the CNT/CB network. Both ternary systems exhibited an improvement in electrical properties during the evolution of the dispersion process.

The modification of the epoxy resin DGEBA increased its fracture toughness. Systems with CNTs exhibited improved mean values of K_{ic} and G_{ic} at 3 h dispersion in most cases. Binary systems with CB exhibited insignificantly enhanced mean values of K_{ic}, with no correlation between that dispersion duration. However, in most of the cases, G_{ic} values decreased or remained stable. Ternary systems exhibited increased K_{ic} as filler percentage and dispersion time increased. Significant improved of G_{ic} was found for CNTs0.5_CB2-III and CNTs0.5_CB2-IV.

Overall, nano- and micro- fillers such as CNTs and CB improved the mechanical properties of epoxies. K_{ic} values, which represent the fracture toughness of the epoxy, increased in all systems, with the most valuable protocol being the CNTs0.5_CB2-IV, due to the synergistic effect that CNTs and CB produce, as mentioned before. In terms of G_{ic}, which represent the maximum energy required to fracture, the most beneficial system was CNTs in all percentages. This could be attributed to the excellent properties of CNTs, such as their high aspect ratio (length-to-diameter ratio).

IS and mechanical measurements revealed a direct correlation between the electrical and mechanical properties of CNTs/CB reinforced epoxy resin, while fractography confirmed the aforementioned results. Various fracture mechanisms were observed in both binary systems (CNTs and CB) such as crack pinning, particle pull-out and deflection. In addition, in ternary systems synergistic effects of the nano- and micro-fillers led to a combination of the above mechanisms.

Author Contributions: G.F.: conceptualization, methodology, analysis, writing—original draft preparation, and editing. K.T.: conceptualization, methodology, analysis, writing—review and editing. L.T.: analysis, writing—review and editing. D.B.: conceptualization, writing—review and editing. A.S.P.: conceptualization, supervision, project administration, review and editing.

Funding: This research has been co-financed by the Operational Program "Human Resources Development, Education and Lifelong Learning" and is co-financed by the European Union (European Social Fund) and Greek national funds.

Acknowledgments: DGEBA, Epikote 828 epoxy resin and Epicure 541 hardener were kindly provided by Dichem Polymers, Greece.

Conflicts of Interest: The authors declare no conflict of interest.

References

1. Sahu, A.; Mondloe, D.S.; Upadhyay, S. A review on thermal properties of epoxy composites as thermal interface material. *Int. Res. J. Eng. Technol.* **2017**, *4*, 579–586.
2. Fiorina, M.; Seman, A.; Castanie, B.; Ali, K.M.; Schwob, C.; Mezeix, L. Spring-in prediction for carbon/epoxy aerospace composite structure. *Compos. Struct.* **2017**, *168*, 739–745. [CrossRef]
3. Sharma, A.; Jang, Y.J.; Kim, J.B.; Jung, J.P. Thermal cycling, shear and insulating characteristics of epoxy embedded Sn-3.0Ag-0.5Cu (SAC305) solder paste for automotive applications. *J. Alloys Compd.* **2017**, *704*, 795–803. [CrossRef]
4. Benea, L.; Mardare, L.; Simionescu, N. Anticorrosion performances of modified polymeric coatings on E32 naval steel in sea water. *Prog. Org. Coat.* **2018**, *123*, 120–127. [CrossRef]
5. Gargano, A.; Pingkarawat, K.; Blacklock, M.; Pickerd, V.; Mouritz, A.P. Comparative assessment of the explosive blast performance of carbon and glass fibre-polymer composites used in naval ship structures. *Compos. Struct.* **2017**, *171*, 306–316. [CrossRef]

6. Grammatikos, S.A.; Paipetis, A.S. On the electrical properties of multi scale reinforced composites for damage accumulation monitoring. *Compos. Part B Eng.* **2012**, *43*, 2687–2696. [CrossRef]
7. Augustin, T.; Karsten, J.; Fiedler, B. Detection and localization of impact damages in carbon nanotube–modified epoxy adhesive films with printed circuits. *Struct. Heal. Monit. Int. J.* **2017**, *15*. [CrossRef]
8. Bekas, D.G.; Paipetis, A.S. Damage monitoring in nanoenhanced composites using impedance spectroscopy. *Compos. Sci. Technol.* **2016**, *134*, 96–105. [CrossRef]
9. Augustin, T.; Grunert, D.; Langner, H.H.; Haverkamp, V.; Fiedler, B. Online monitoring of surface cracks and delaminations in carbon fiber/epoxy composites using silver nanoparticle based ink. *Adv. Manuf. Polym. Compos. Sci.* **2017**, *3*, 110–119. [CrossRef]
10. Govorov, A.; Wentzel, D.; Miller, S.; Kanaan, A.; Sevostianov, I. Electrical conductivity of epoxy-graphene and epoxy-carbon nanofibers composites subjected to compressive loading. *Int. J. Eng. Sci.* **2018**, *123*, 174–180. [CrossRef]
11. Wentzel, D.; Miller, S.; Sevostianov, I. Dependence of the electrical conductivity of graphene reinforced epoxy resin on the stress level. *Int. J. Eng. Sci.* **2017**, *120*, 63–70. [CrossRef]
12. Mittal, G.; Dhand, V.; Rhee, K.Y.; Park, S.J.; Lee, W.R. A review on carbon nanotubes and graphene as fillers in reinforced polymer nanocomposites. *J. Ind. Eng. Chem.* **2015**, *21*, 11–25. [CrossRef]
13. Hernández-Pérez, A.; Avilés, F.; May-Pat, A.; Valadez-González, A.; Herrera-Franco, P.J.; Bartolo-Pérez, P. Effective properties of multiwalled carbon nanotube/epoxy composites using two different tubes. *Compos. Sci. Technol.* **2008**, *68*, 1422–1431. [CrossRef]
14. Baltzis, D.; Bekas, D.G.; Tzachristas, G.; Parlamas, A.; Karabela, M.; Zafeiropoulos, N.E.; Paipetis, A.S. Multi-scaled carbon reinforcements in ternary epoxy composite materials: Dispersion and electrical impedance study. *Compos. Sci. Technol.* **2017**, *153*, 7–17. [CrossRef]
15. Wode, F.; Tzounis, L.; Kirsten, M.; Constantinou, M.; Georgopanos, P.; Zafeiropoulos, N.E.; Avgeropoulos, A.; Stamm, M. Selective localization of multi-wall carbon nanotubes in homopolymer blends and a diblock copolymer. Rheological orientation studies of the final nanocomposites. *Polymer* **2012**, *53*, 4438–4447. [CrossRef]
16. Liebscher, M.; Tzounis, L.; Pötschke, P.; Heinrich, G. In fluence of the viscosity ratio in PC/SAN blends fi lled with MWCNTs on the morphological, electrical, and melt rheological properties. *Polymer* **2013**, *54*, 6801–6808. [CrossRef]
17. Tzounis, L.; Debnath, S.; Rooj, S.; Fischer, D.; Mäder, E.; Das, A.; Stamm, M.; Heinrich, G. High performance natural rubber composites with a hierarchical reinforcement structure of carbon nanotube modified natural fibers. *Mater. Des.* **2014**, *58*, 1–11. [CrossRef]
18. Papageorgiou, D.G.; Tzounis, L.; Papageorgiou, G.Z.; Bikiaris, D.N.; Chrissa, K. b-nucleated propylene-ethylene random copolymer filled with multi-walled carbon nanotubes: Mechanical, thermal and rheological properties. *Polymer* **2014**, *55*, 3758–3769. [CrossRef]
19. Tzounis, L.; Herlekar, S.; Tzounis, A.; Charisiou, N.D.; Goula, M.; Stamm, M. Halloysite Nanotubes Noncovalently Functionalised with SDS Anionic Surfactant and PS-b-P4VP Block Copolymer for Their Effective Dispersion in Polystyrene as UV-Blocking Nanocomposite Films. *J. Nanomater.* **2017**, *2017*, 3852310. [CrossRef]
20. Pötschke, P.; Liebscher, M.; Gärtner, T.; Tzounis, L.; Mic, M.; Stamm, M.; Heinrich, G.; Voit, B. Influence of the MWCNT surface functionalization on the thermoelectric properties of melt-mixed polycarbonate composites. *Composit. Sci. Technol.* **2014**, *101*, 133–138.
21. Liebscher, M.; Petra, P.; Voit, B.; Heinrich, G.; Stamm, M. In fluence of a cyclic butylene terephthalate oligomer on the processability and thermoelectric properties of polycarbonate/MWCNT nanocomposites. *Polymer* **2014**, *55*, 5381–5388.
22. Tzounis, L.; Pegel, S.; Zafeiropoulos, N.E.; Avgeropoulos, A.; Paipetis, A.S.; Stamm, M. Shear alignment of a poly (styrene-butadiene-styrene) triblock copolymer/MWCNT nanocomposite. *Polymer* **2017**, *131*, 1–9. [CrossRef]
23. Tzounis, L.; Hegde, M.; Liebscher, M.; Dingemans, T.; Petra, P. All-aromatic SWCNT-Polyetherimide nanocomposites for thermal energy harvesting applications. *Compos. Sci. Technol.* **2018**, *156*, 158–165. [CrossRef]
24. Li, C.; Thostenson, E.T.; Chou, T.W. Dominant role of tunneling resistance in the electrical conductivity of carbon nanotube-based composites. *Appl. Phys. Lett.* **2007**, *91*, 223114. [CrossRef]

25. Stauffer, D.; Ammon, A. *Introduction to Percolation Theory*, 2nd ed.; Taylor and Francis: New York, NY, USA, 1994.
26. Burmistrov, I.; Gorshkov, N.; Ilinykh, I.; Muratov, D.; Kolesnikov, E.; Anshin, S. Improvement of carbon black based polymer composite electrical conductivity with additions of MWCNT. *Compos. Sci. Technol.* **2016**, *129*, 79–85. [CrossRef]
27. Fenner, J.S.; Daniel, I.M. Hybrid nanoreinforced carbon/epoxy composites for enhanced damage tolerance and fatigue life. *Compos. Part A Appl. Sci. Manuf.* **2014**, *65*, 47–56. [CrossRef]
28. Ayatollahi, M.R.; Shokrieh, M.M.; Shadlou, S.; Kefayati, A.R.; Chitsazzadeh, M. Mechanical and Electrical Properties of Epoxy/Multi-walled Carbon Nanotube/Nanoclay Nanocomposites. *Iran. Polym. J.* **2011**, *20*, 835–843.
29. Zakaria, M.R.; Akil, H.M.; Kudus, M.H.A.; Kadarman, A.H. Improving flexural and dielectric properties of MWCNT/epoxy nanocomposites by introducing advanced hybrid filler system. *Compos. Struct.* **2015**, *132*, 50–64. [CrossRef]
30. Baltzis, D.; Orfanidis, S.; Lekatou, A.; Paipetis, A.S. Stainless steel coupled with carbon nanotube-modified epoxy and carbon fibre composites: Electrochemical and mechanical study. *Plast. Rubber Compos.* **2016**, *45*, 95–105. [CrossRef]
31. Gkikas, G.; Barkoula, N.; Paipetis, A.S. Composites: Part B Effect of dispersion conditions on the thermo-mechanical and toughness properties of multi walled carbon nanotubes-reinforced epoxy. *Compos. Part B* **2012**, *43*, 2697–2705. [CrossRef]
32. Hardis, R.; Jessop, J.L.P.; Peters, F.E.; Kessler, M.R. Composites: Part A Cure kinetics characterization and monitoring of an epoxy resin using DSC, Raman spectroscopy, and DEA. *Compos. Part A* **2013**, *49*, 100–108. [CrossRef]
33. Han, Y.; Wang, J.; Zhang, H.; Zhao, S. Sensors and Actuators A: Physical Electrochemical impedance spectroscopy (EIS): An efficiency method to monitor resin curing processes. *Sens. Actuators A. Phys.* **2016**, *250*, 78–86. [CrossRef]
34. Bekas, D.G.; Paipetis, A.S. Study of the Effect of Damage on the Electrical Impedance of Carbon Nanotube Reinforced Epoxy Nanocomposites. *J. Sens.* **2015**, *2015*, 805303. [CrossRef]
35. Bekas, D.G.; Gkikas, G.; Maistros, G.M.; Paipetis, A.S. On the use of dielectric spectroscopy for the real time assessment of the dispersion of carbon nanotubes in epoxy. *RSC Adv.* **2016**, *6*, 78838–78845. [CrossRef]
36. Bouchard, J.; Cayla, A.; Devaux, E.; Campagne, C. Electrical and thermal conductivities of multiwalled carbon nanotubes-reinforced high performance polymer nanocomposites. *Compos. Sci. Technol.* **2013**, *86*, 177–184. [CrossRef]
37. Socher, R.; Krause, B.; Boldt, R.; Hermasch, S.; Wursche, R.; Pötschke, P. Melt mixed nano composites of PA12 with MWNTs: Influence of MWNT and matrix properties on macrodispersion and electrical properties. *Compos. Sci. Technol.* **2011**, *71*, 306–314. [CrossRef]
38. ASTM Standards. *D5045-Standard Test Methods for Plane-Strain Fracture Toughness and Strain Energy Release Rate of Plastic Materials*; ASTM Inernational: West Conshohocken, PA, USA, 1999; pp. 1–9.
39. Zhang, M.Q.; Yu, G.; Zeng, H.M.; Zhang, H.B.; Hou, Y.H. Two-step percolation in polymer blends filled with carbon black. *Macromolecules* **1998**, *31*, 6724–6726. [CrossRef]
40. Science, C.; Quaresimin, M.; Zappalorto, M.; Chandrasekaran, S.; Livermore, L. Toughening mechanisms in polymer nanocomposites: From experiments to modelling. *Compos. Sci. Technol.* **2016**, *123*, 187–204.